

## Electromagnetic design of a new radial flux permanent magnet motor

Ibtissam Bouloukza

University of 20 août 1955, Department of Electrical Engineering, LRPCSI Laboratory, Skikda, Algeria, boulekza\_ibtm@yahoo.fr, orcid.org/0000-0001-6976-973X

Mourad Mordjaoui

University of 20 août 1955, Department of Electrical Engineering, LRPCSI Laboratory, Skikda, Algeria, mordjaoui\_mourad@yahoo.fr, orcid.org/0000-0002-5195-6016

Erol Kurt

Gazi University, Faculty of Technology, Department of Electrical and Electronic Engineering, Ankara, Turkey, ekurt52tr@yahoo.com, orcid.org/0000-0002-3615-6926

Güngör Bal

Gazi University, Faculty of Technology, Department of Electrical and Electronic Engineering, Ankara, Turkey, gungorbal@gmail.com, orcid.org/0000-0002-0564-5903

Coşkun Ökmen

General Directorate of State Airports Authority, Department of Aviation Electricity, Kars Airport, Kars, Turkey, okmen.coskun@gmail.com, orcid.org/0000-0003-4227-5873

Arrived: 23.02.2018 Accepted: 15.03.2018 Published: 31.03.2018

**Abstract:** This paper proposes a new design study for a three-phase permanent magnet motor. The radial flux machine has 12 pole type magnets in its rotor internally and a surface mounted stator has 36 coils surrounding the cores. Initially, a magnetostatic study has been performed, and then a 2D transient finite element analysis has been realized in order to verify the new design concept. Then, a harmonic analysis is performed to see the harmonic impact on the design performance and achieving a good prototype. The new-designed machine is promising since it gives symmetrical field structure under operation and the electromagnetic torques and current waveforms characteristics are good for different angular spreading of magnet.

**Keywords:** Permanent magnet machine, Electromagnetic design, Radial flux, 2D FEM, Harmonic analysis,

Cite this paper as: Bouloukza, I., Mordjaoui, M., Kurt, E., Bal, G., Ökmen, C, *Electromagnetic design of new radial flux permanent magnet motor. Journal of Energy Systems* 2018; 2(1): 13-27, DOI: 10.30521/jes.397836

## 1. INTRODUCTION

The advances in engineering and technology have contributed to many areas such as machine control, electrical vehicles, communication, military defense technology and renewable energy. Among them, efficient motor design has become most important one, since the moving parts of robots, vehicles and industrial production line devices mostly require motors with different designs and structures. They have been either permanent magnet (PM) machines or magnet-free machines; they should obey the rules of magnetic force excitation.

In a last few decades, the electric usage in various applications has been intensely increased. Indeed, that demand has been multiplied for a more energized world, where the fossil fuels are replaced by other sources [1-2]. The synchronous PM machines have a great interest in the industrial world [3-7]. That enforces the engineers to design better machines according to their operation aims: better dynamic performance, higher efficiency, lower power consumption, higher torque per volume, etc. [8-13] can be counted. The structure of a PM machine gives superiorities for the control of their speed and position. In fact, the armature field can be precisely controlled and it can be always synchronized with the rotor. Thus, it becomes convenient to implement precise position control and speed on PM machines. Several structure types of synchronous PM machines are possible. Indeed, these varieties are related with magnets and their arrangements at the rotor unit. The rare earth Neodymium (NdFeB) magnets, which have the largest flux densities among the PMs can provide the best magnetic force performance compared to those made by conventional magnets [9-11]. Depending on the magnet topology in the rotor, PM machines can be classified as radial flux and axial flux machines [12-13]. While the PMs are arranged in the inner cylinder on the rotor unit in the radial flux machines, so that the torque is produced from magnetic flux that is perpendicular to the rotor shaft [14-15], the magnets are arranged on a disk, so that the magnetic flux flowing parallel to the shaft produces the torque in the axial flux machine [14-18].

The shape of the signal of the electromotive force (EMF) of the machine depends very much on the type of winding used. So, in the case of PM machine, we have to look for a winding that gives the closest signal to a sinusoid. The majority of machines were designed with distributed stator windings or concentration stator winding. The use of concentration winding was not popular due to a poor torque to magnetomotive force (MMF) ratio. However, in the early 21st century, some authors [19-21] proved that by an appropriate choice of slot and pole combination, as consequence, cogging torque can also be reduced. The present design uses concentrated double-layer windings. This type of coil arrangements exhibits better properties compared to the traditional distributed windings. The machines that use this type of winding can have each coil wounded around one stator tooth. This makes the machine winding process, in principle and in practice, easy and in expensive, and consequently, the machine type is an interesting option in mass production.

Since the present design uses the finite element analysis (FEA), brief information can be mentioned about the simulation method. Strictly speaking, this method is based on the evaluation of the field values, calculated at the finite elements on the meshed structure. The method is frequently used in electromagnetic and mechanical simulations due to its high accuracy. The Maxwell equations can be solved for both steady-state and transient operations [16], however it may require much simulation time for transient solutions in order to drive the system to its actual state. Therefore optimal mesh number and time step are critical parameters for a simulation. A compact 2D model can lead to a much shorter solutions due to the smaller meshed area and then it can be easily transformed into a 3D solution. In the recent simulation packages, the FEA covers the optimization tools in order to seek the most appropriate parameters for a design. In detail, the quantities to be optimized can be saturation, induced currents, hysteresis, air gap, winding volume, etc. [23-25].

The finite element analysis gives very accurate results with short computation time using the magnetodynamic solution type. However, the harmonics problem cannot be neglected because the rotor motion must be taken into account. Most of the design procedures used for electrical machines are focused to achieving a better performance with the lowest possible harmonic content.

The present design reports the electromagnetic findings on a new PM motor in terms of FEA. The study includes both 2D simulations and transient solutions with harmonic analysis. Although the design has been continuing, the preliminary findings on magnetic fluxes, voltages, currents and mechanical torques are presented.

## 2. DESIGN

The starting configuration for the proposed PM motor is shown in Fig. 1. In this 2D appearance, the motor has been drawn in master-slave representation in a 60 degrees surface and can be simulated over a full-cycle surface, too. The PM motor has an inner rotor and an outer stator unit. In that structure, the inner rotor includes a shaft from stainless steel at the middle, a surface mounted cylindrical core over that stainless steel, and the magnets have been embedded into the rotor core for better flux distribution from rotor to stator. The machine has 12 salient poles, and the magnets in total and they are oriented towards the air gap.

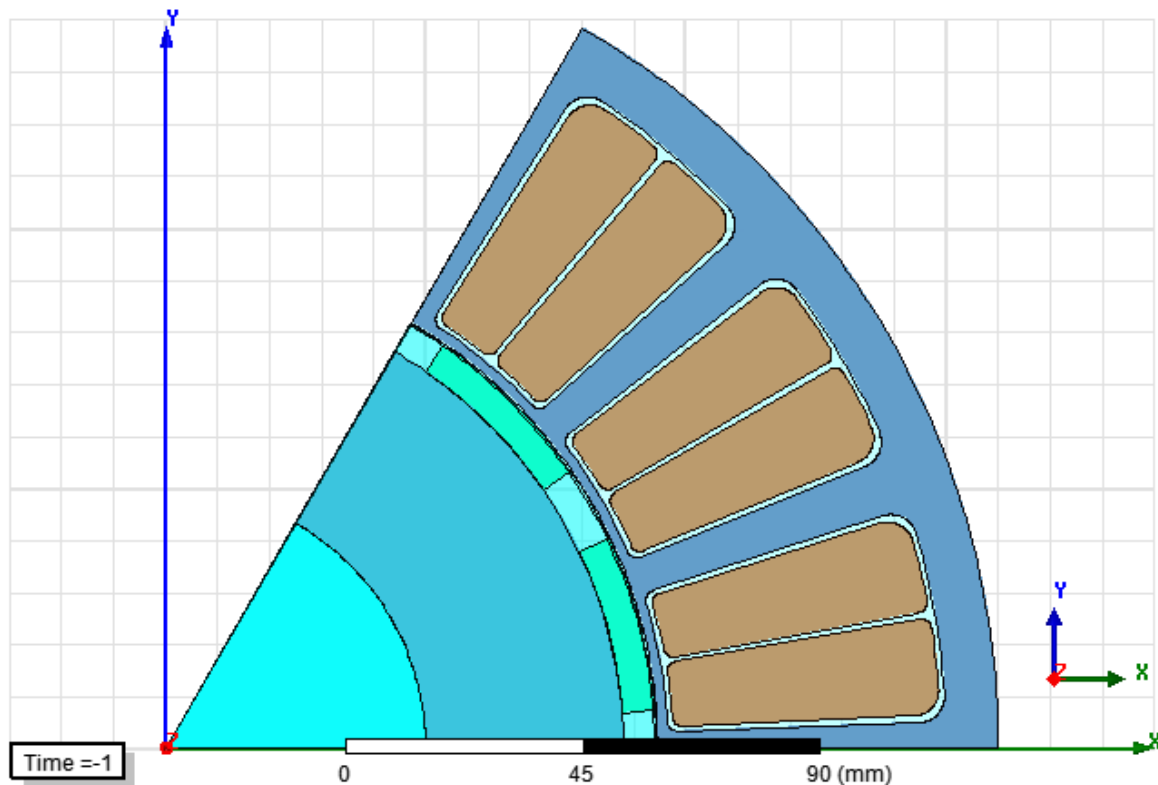


Figure 1. 2D configuration of the proposed motor.

In the stator part (Fig. 1), a double winding system is positioned in each slot to provide a two-fold excitation. In that context, the stator has 18 slots in total and the windings are distributed to form a three-phase excitation on the machine operation. A detailed geometry is presented in Table 1.

Table. 1. Design parameters of the machine

Components	Features
Inner radius of rotor	55 mm
Outer radius of rotor	94 mm
Inner radius of stator	94.5 mm
Outer radius of stator	160 mm
Phase number	3
Coil number	36
Magnet pole number	12
Magnet thickness	6 mm
Stator core material	M22-29G
Rotor core material	Ferrite
Magnet material	NdFe30
Shaft material	Stainless steel
Wire material	Copper
Core type	Radially laminated
Air gap	0.5 mm

Briefly it can be stated that the present machine has a 64 cm diameter and the length can be increased in accordance with the desired power scale. Windings have a radial length of 2 cm. Thus the excitation from the windings can be transmitted to machine better to provide a good mechanical torque.

### 2.1. Excitation and Winding Connections

In order to excite the windings, a three-phase excitation is provided as presented in Fig. 2.

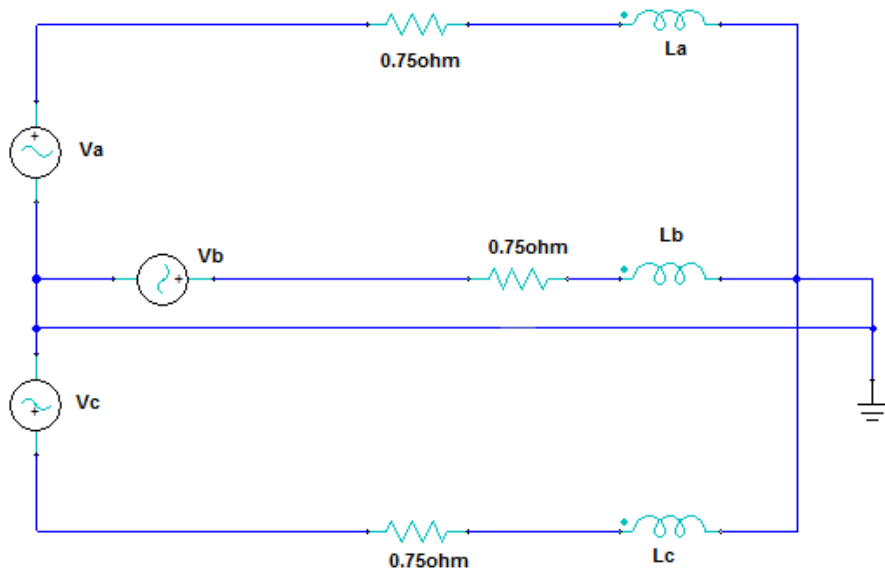


Figure 2. Three phase external excitation circuit for the stator windings.

This type excitation can provide us a good media to compute the transient solutions. Each phase windings can be fed by  $V_i$  voltages having a certain phase and each phase has modeled with stranded coils, and a resistance of  $R=0.75\ \Omega$ . However, other external circuits can also be applied to excite the machine. In our simulations, we have adjusted the voltage for one phase “127 Volt”. The external circuit connections allow us to simulate the operating conditions of the motor with the motor’s real power supply connections.

The type of stator winding used in an electrical machine is determined by the number of slots  $Q_s$ , the number of poles  $p$ , and the number of phases  $m$ . These parameters of the machine determine  $q$ , the number of slots per pole and phase as Eq. (1):

$$q = \frac{Q_s}{mp} \quad (1)$$

In the concentrated winding, the opposite polarity of the corresponding phase coil is located in the next slot as shown in Fig.3. Depending on the type of stator winding, they can be single-layered or double-layered stator. The choice depends on the desired machine performance characteristics. Single-layer winding creates high self inductance and low mutual inductance which leads to better fault-tolerant capability. On the other hand, double-layer winding has lower air gap MMF harmonic components, thereby resulting in smaller torque ripples and lower magnet eddy current losses [19,21]. In this paper, the winding layouts are classified as double-layer as shown in Fig. 3.

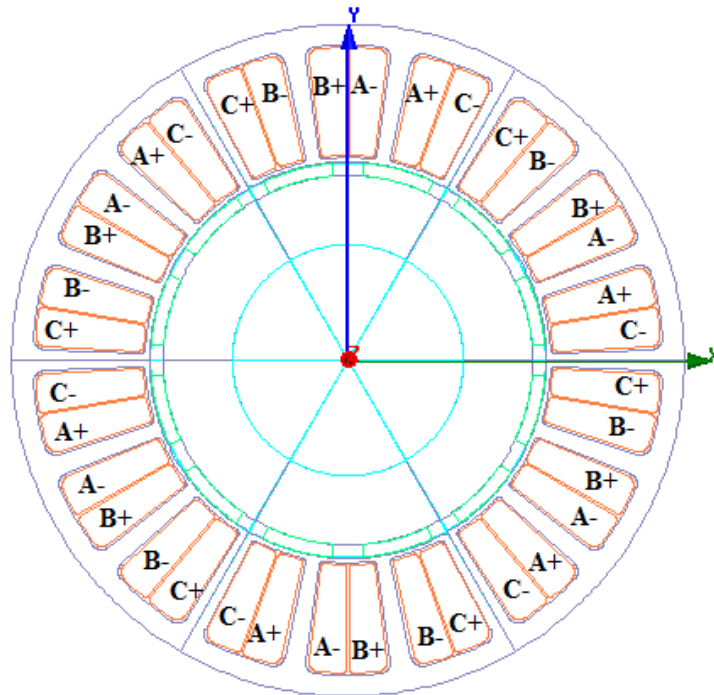


Figure 3. Double-layer concentrated winding.

## 2.2. Electromagnetic quantities

According to general laws of electromagnetic, energy conservation can be applied to estimate the actuator performance in terms of global quantities. The electromagnetic quantities such as currents in the phases and magnetic fields can be examined through the simulations and the motor performances can be determined. However, before the transient tests, the maximal flux level should be determined throughout the flux path in order to prove the optimal thickness in core slots.

In such machines, the electromagnetic torque and power relation can be summarized as Eq. (2):

$$P_{em}(t) = \Gamma_{em}(t)\omega \quad (2)$$

Here  $\Gamma_{em}$  is the electromagnetic torque of the machine and  $\omega$  represent the rotational speed in radians per seconds. The electromagnetic power is then expressed simply by the sum over all phases at a constant rotational speed, thereby the electromagnetic torque is determined by Eq. (3):

$$\Gamma_{em}(t) = \frac{1}{\omega} \sum_{k=1}^3 v_k(t) i_k(t) = \frac{2}{\omega} vi \quad (3)$$

Where  $v$  and  $i$  are EMF and the current in a phase, respectively. The current in each phase is written as Eq. (4):

$$i = \frac{\Gamma_{em}\omega}{2v} \quad (4)$$

The EMF is calculated from the variation of flux passing through a coil using the Faraday law. When the rotor rotates in a polar pitch (i.e.  $\pi/p$ ), a magnet takes the place of an adjacent magnet and the flux  $\varphi$  in the coil is then reversed as Eq. (5):

$$v = \frac{N_{ph}}{2} \frac{d\varphi}{d\theta} \frac{d\theta}{dt} = N_{ph} \frac{\varphi}{\pi/p} \quad (5)$$

The EMF is calculated from the variation of flux passing through a coil using the Faraday law. When the rotor rotates in a polar pitch (i.e.  $\pi/p$ ), a magnet takes the place of an adjacent magnet and the flux  $\varphi$  in the coil is then reversed as Eq. (5):

$$e = n_s k_w \frac{d\varphi}{dt} \quad (6)$$

That process generates the EMF depending on the flux variation. Here  $N_{ph}$  is the number of conductors per phase (the number of conductors is equal to twice the number of turns) and  $\varphi$  is the unit flux corresponding to a turn in a phase. Unlike distributed windings, concentrated windings perform a winding factor below the unit. This means that due to the different distribution of slots  $Q_s$  and poles  $p$ , the electromotive force (EMF) induced in each phase is not the addition of the absolute value of the EMF induced in each conductor, since they are phase shifted. According to the Faraday's induction law:

$$\varphi = B_e S_p \quad (7)$$

Where  $e$  is the electromotive force induced,  $n_s$  is the number of turns per slot, and  $k_w$  is the fundamental winding factor. Then a function for the flux over the air gap can be written as Eq. (7):

$$\Gamma_{em} = N_{ph} I B_e \frac{S_e}{\pi} \quad (8)$$

where  $S_p$  is the surface of a magnetic pole and  $B_e$  is the mean value of the induction in the air gap, respectively.

By combining Eqs. (3,4) and (7), the torque expression is transformed into Eq. (8):

$$N_{ph} = \left( v \left( \frac{U}{B_e D_s L_m \omega \frac{N_{te}}{3}} \right) + 1 \right) \frac{N_{te}}{3} \quad (9)$$

Where  $v$  is the integer part,  $U$  is the supply voltage,  $N_{te}$  is the total number of slot,  $D_s$  is the bore diameter and  $L_m$  is the length of iron. For radial flux PM machines, the total air gap area is expressed as Eq. (10):

$$S_e = \pi D_s L_m \quad (10)$$

Considering Eqs. (8,9), the current in a phase is expressed as a function of the induction in the air gap, the electromagnetic torque and the dimensions of the machine as Eq. (11):

$$I = \frac{\Gamma_{em}}{N_{ph}B_e D_s L_m} \quad (11)$$

### 2.3. Material parameters

The stator and the outer part of the rotor are made of a soft ferromagnetic material unlike the magnets, which are made of hard ferromagnetic materials. Fig. 4 presents the  $B-H$  curve of the magnet material (i.e. NdFeB). That material has a higher residual flux density and a higher coercive force compared to other magnet materials. Generally, the temperature limitation for PMs is under  $120^\circ$  due to their temperature-dependent demagnetization curves. In the recent studies, that limit has been raised to  $180^\circ\text{C}$  for the alloy mixture Nb specimens.

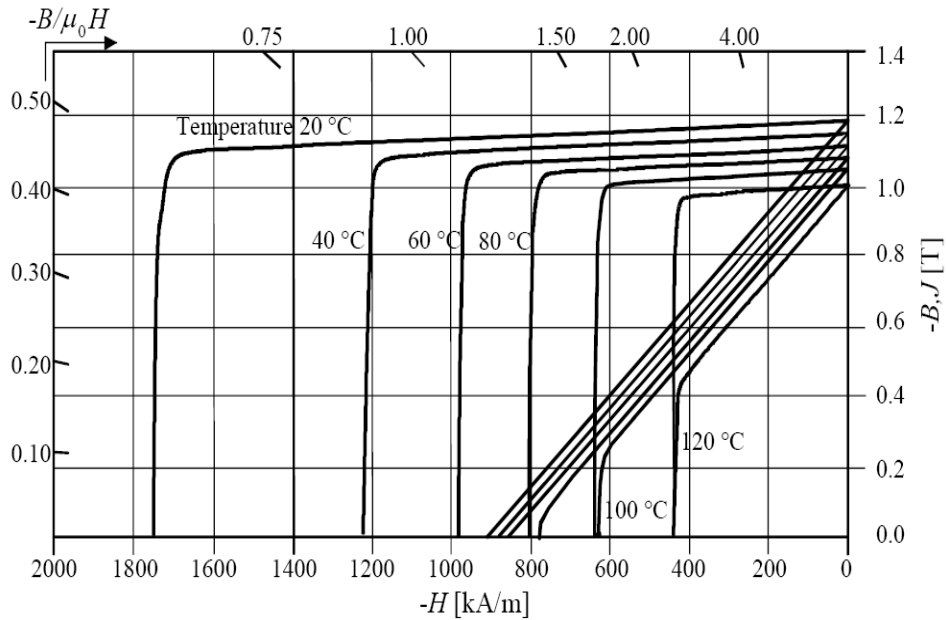


Figure 4. Material characteristics of a NdFeB specimen [26].

Table 2 summarizes the motor ratings in terms of its power, rated voltage and frequency. For our preliminary design, 3 kW power has been considered as sufficient, where as the length of the machine can be increased and that can lead to higher power values.

Table 2. Motor ratings

Ratings	Values
Output power	3 kW
Rated voltage	127 V
Frequency	60 Hz

### 3. RESULTS and DISCUSSION

#### 3.1. Finite Element Analysis

In the present design, FEA starts with the definition of the machine geometry and the boundary conditions for fields and determination of mesh structure. The radial flux motor has a cylindrical geometry as usual and the material properties of components such as magnetic permeability, dielectric constant and current density are key points to define at the input geometry. In terms of boundary conditions, Dirichlet conditions, where the value of the solution field is held constant and Neumann conditions, where the derivative of the solution field is set to zero, are key definitions. Especially in magnetic problems, the Dirichlet condition forces magnetic flux lines parallel to the boundary, whereas the Neumann condition forces the flux lines perpendicular to the boundary. Besides, a periodicity for solutions can be used to define a single pole pair of a multi-pole machine by setting boundaries on opposite sides of the geometry to be equal.

To predict the performance of the machine accurately, a 2D finite element analysis is applied to the new design obtained by the equivalent magnetic circuit. In order to assess the dynamic performance of the proposed flux control, the machine runs from steady state to 300 rpm. However, to achieve the overall feature of the machine, higher speeds should also be examined as will be performed for future works. In the present work, the global mesh structure is defined as in Fig. 5.

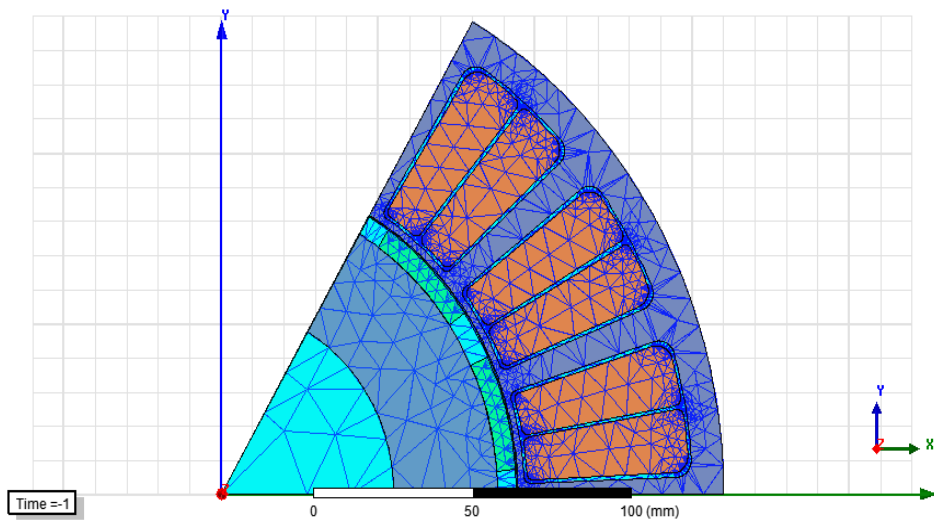


Figure 5. The mesh structure of the proposed machine.

The FEA model has been utilized to explore the potential field issues to provide the functions such as flux density  $B$  and flux  $\phi$ . The results of the magnetostatic solutions and flux density lines distribution are shown in Fig. 6(a,b). While the vector representation is depicted in Fig. 6(a), Fig. 6(b) gives the magnitudes of the flux density. According to these analyses, it has been proven that especially the fields in slot sides are acceptable with the current thickness value of core teethes. These regions have the maximal values of flux densities around 1.8 T, which is sufficient for the machine. Only the value increases up to 2 T for the inner edges of slots and that is in the limit.

Since the values for each node can be known, the geometry (i.e. thickness) of the stator teeth can be optimized easily. Note that the simulation has been calculated for the extremely small air gap (i.e. 0.5 mm), and in the optimized conditions (i.e. 1.5 mm air gap value), the field values should be decreased further. For the relation of magnetic flux density and air gap, we refer to one of our earlier studies [27].

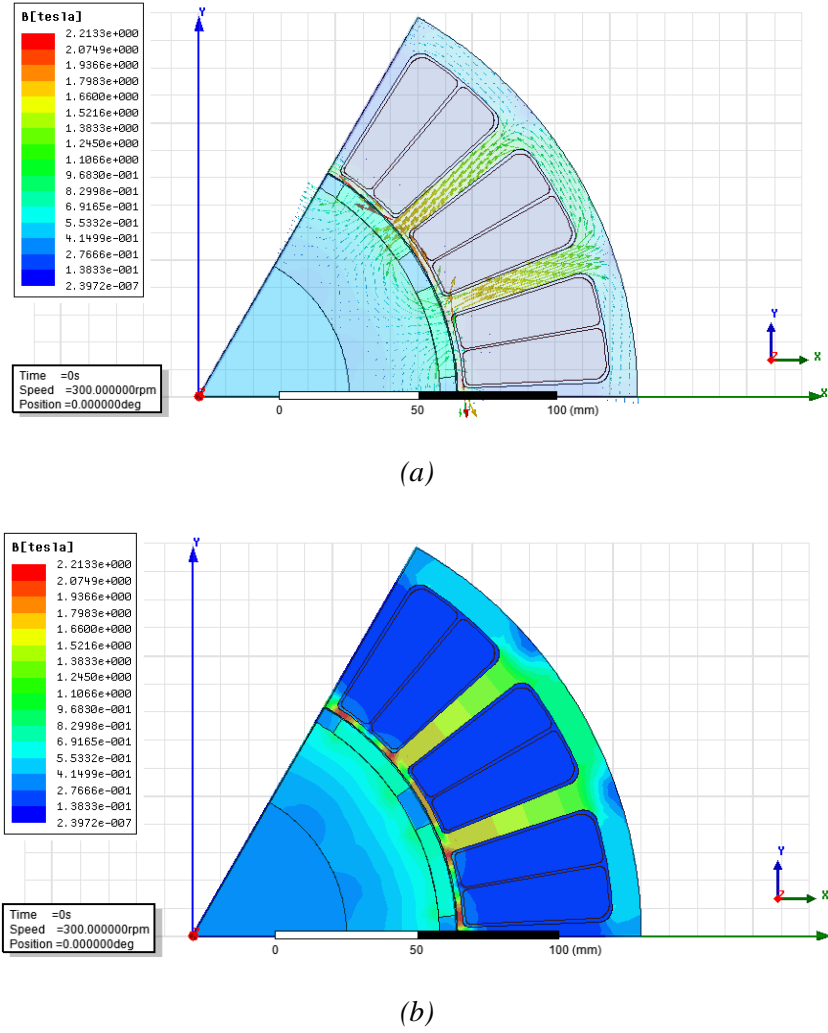


Figure 6. (a) The vector representation of the magnetic flux density, (b) The strength of the magnetic flux density.

### 3.2. Transient case and harmonic analysis

In the transient case, initially the excitation formula should be stated as Eq. (12-13):

$$V = V_{max} * \sin(\omega_{rad} * t + \theta_0) \quad (12)$$

$$\omega_{rad} = \left(360 * \vartheta_{rpm} * \frac{p}{60}\right) * \frac{\pi}{180} \quad (13)$$

Note that the motor is excited with a balanced three-phase connection and a sinusoidal excitation is applied as general. At each time step, the phases have a 120-degree shift between the each as usual. In the formula above,  $V_{max}$ ,  $\omega_{rad}$ ,  $\vartheta_{rpm}$  and  $p$  represent maximum value of winding voltage, pulsation of the excitation, speed of the motor in rpm and number of pair of poles respectively.

Transformation of periodic curves into Fourier analysis to determine the harmonic of the waveforms is widely used in characteristics of electrical machine [28] or others [29]. We perform a harmonic analysis of performance of the PM machine. The analysis of the PM machine is discarded since we know that,

for this type of machine, the signal of its magnetic fluxes, voltages, currents and mechanical torques is rich in high order harmonics.

### 3.3. The Back EMF

The back EMF in windings *B* and *C* can be easily obtained from that of winding *A* by 120 and 240 electrical degrees offset, respectively. Fig. 7 shows the back EMF and its harmonic spectrum at 300 rpm for the no-load case. At the speed 300 rpm, the maximal peak to peak voltage is found as 126 V. The waveforms are obtained as sinusoidal and the phase shifts are preserved perfectly for the three phases.

The EMF waveform is a periodic electrical signal by  $2\pi$  period that admits an asymmetry with respect to the abscissae, as well as the signal of the EMF is marred by harmonics of higher ranks even if the fundamental prevails. This is due to the slot effect on the EMF signal. The harmonic analysis gives us a glimpse of the signal quality of the EMF.

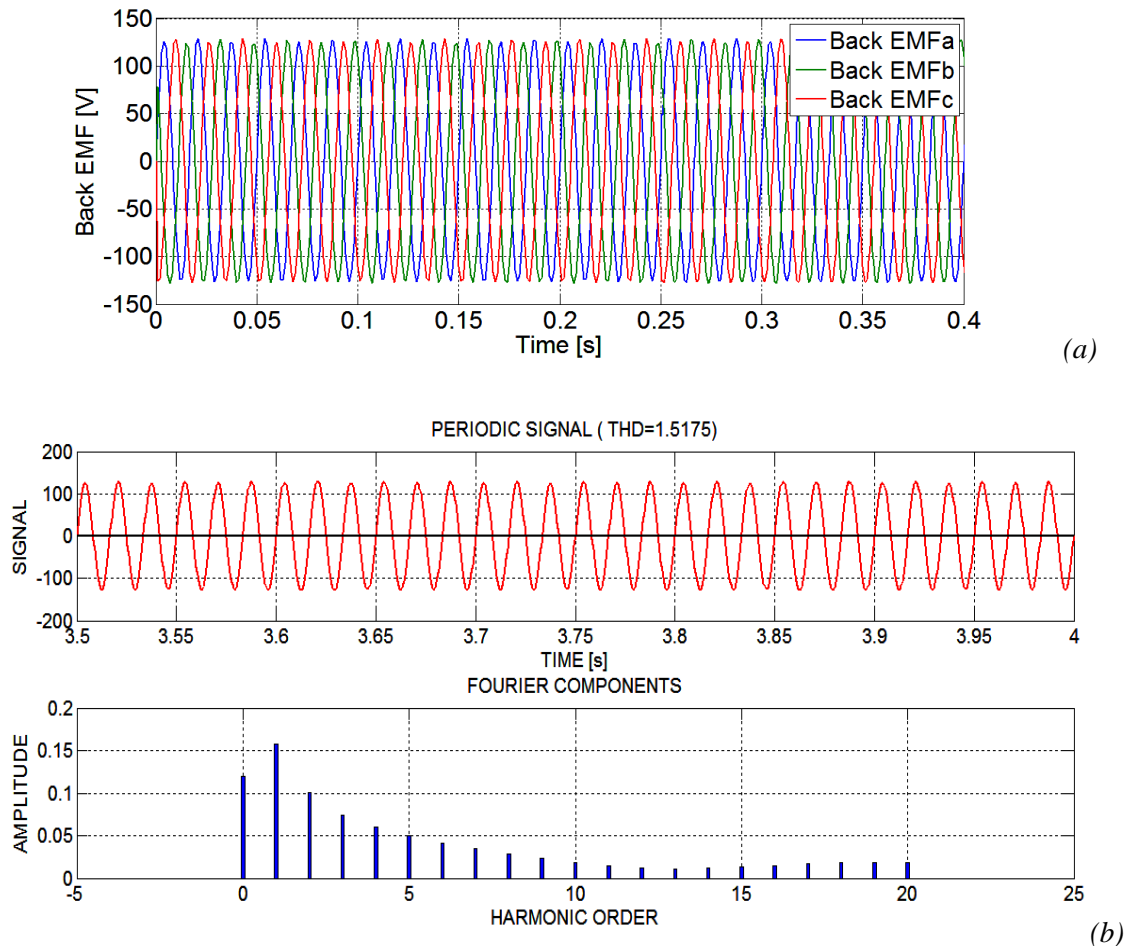


Figure 7. The back EMF waveform at the rotor speed 300 rpm for (a) Total simulation time (phase A, B, C) and (b) Detailed overview and harmonics (phase A, no-load, 127 V, 300 rpm).

Simulations have been carried out for different speed as seen in Fig. 8. According to the transient simulations, the maximal amplitudes increase to 129 V for 1200 rpm. It is noted that the rotor speed and the amplitude of back EMF have a linear relation as usual.

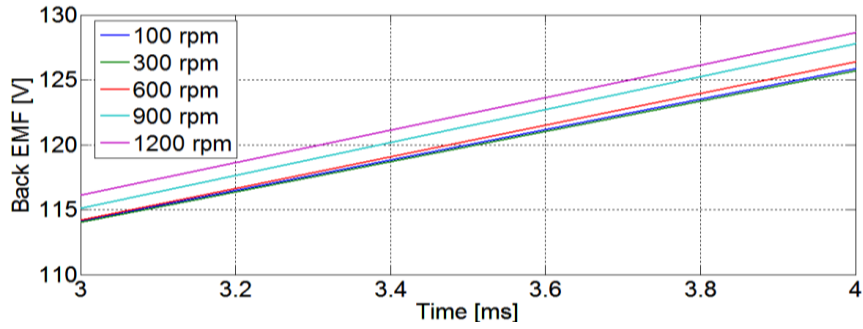


Figure 8. The back EMF versus time for different rotor speeds.

### 3.4. The Current

For a new machine, the current profile becomes very important in order to determine the wire cross section at the windings and the losses. The currents flowing through the phases and its harmonic spectrum are plotted in Fig. 9 at 300 rpm. The maximal currents amplitude are simulated as 8.5 A at 300 rpm. These currents are sufficient for the wires to carry and also the phase shifts are observed very well. This indicates that the machine design is stable for each phase at 300 rpm.

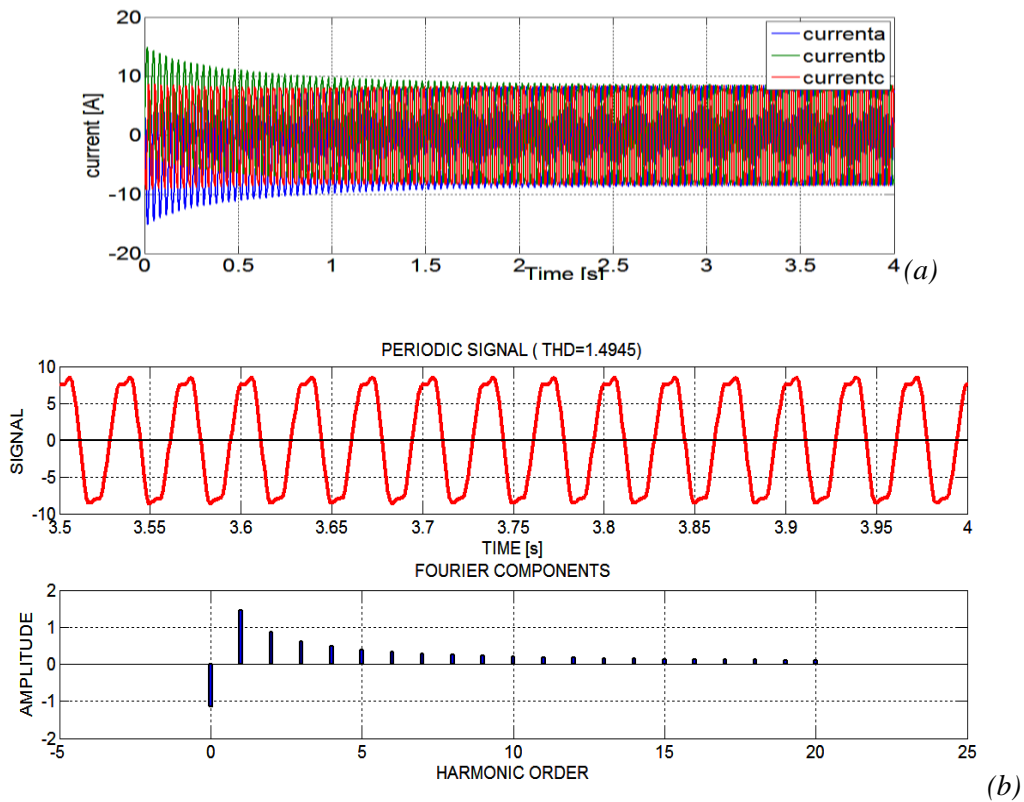


Figure 9. Current waveform at the speed 300 rpm for (a) Total simulation time (phase A, B, C) and (b) Detailed overview and harmonics (phase A, no-load, 127 V, 300 rpm).

The currents flowing through the serial connected windings of phase A are plotted in Fig. 8. Initially, it is stated that the waveforms are identical for each phase. In the minimal and maximal parts of the current waveforms, there exist weak distortions from the ideal sinusoidal signal. The results of performing Fourier harmonic decompositions on one phase of current are plotted in Fig. 9 as a function of harmonic order.

### 3.5. The Magnetic Flux

Fig. 10 shows the magnetic flux characteristics and its harmonic spectrum of the motor for no-load conditions. After the transient solutions, three phases show the same flux value with  $\pm 0.36$  Wb for 300 rpm. Note that the sinusoidal appearance in waveform gives a clue for the induced phase voltage. The phase differences over the phases are also clear.

The harmonic spectrum of the magnetic flux is shown in Fig. 10. It can be seen that other than the fundamental component, the only spatial components that have significant values:  $\leq 10$  of harmonic order.

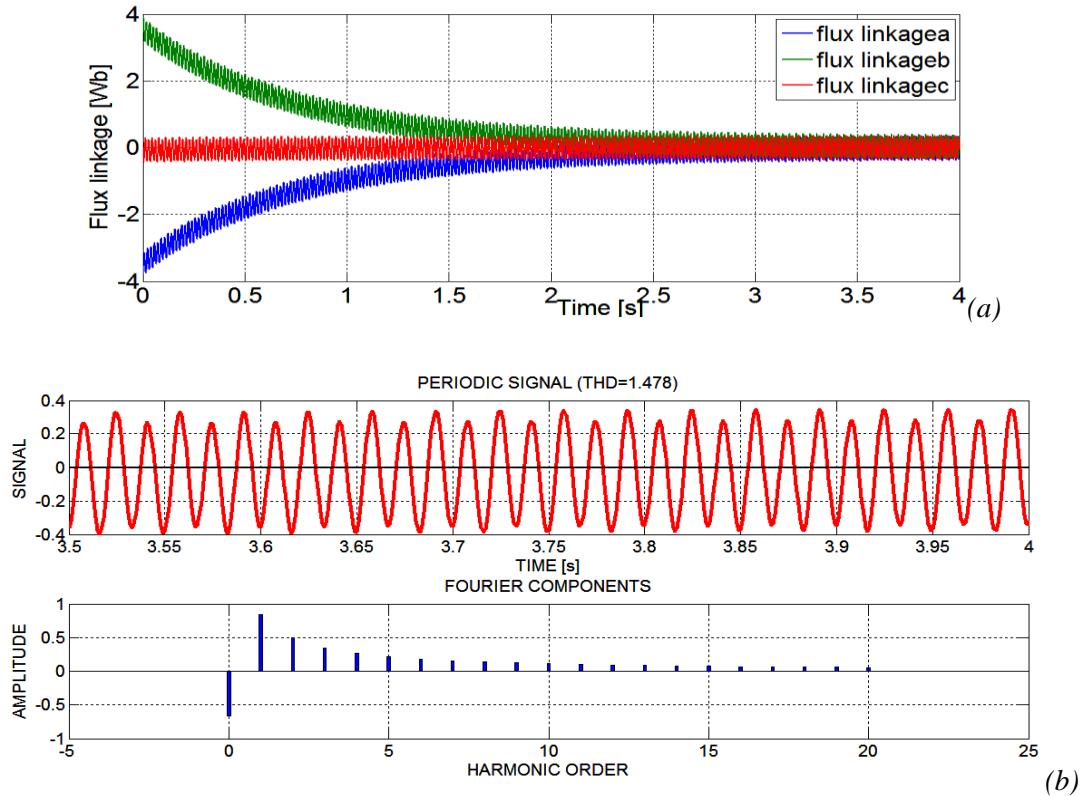


Figure 10. Magnetic fluxes at 300 rpm during (a) Total simulation time(phase A, B, C) and (b) Detailed overview and harmonics (phase A, no-load, 127 V, 300 rpm).

### 3.6. The Mechanical Torque

The preliminary simulations end with the mechanical torque findings as shown in Fig. 11. The overall simulation on mechanical torque variation is plotted in Fig. 11(a), whereas the last part of the entire simulation is depicted in Fig. 11(b) for 300 rpm. According to those findings, the machine can produce the torque average value of 65 Nm, however the torque curve has negative and positive torque values since the simulation has been realized under no-load condition. The presence of a regular oscillation can be observed as a result of the magnetic force depending on the rotor position.

In the steady state, the torque reaches to a nominal value with a regular oscillation and that is observed due to the saturation effect and the geometry of the machine.

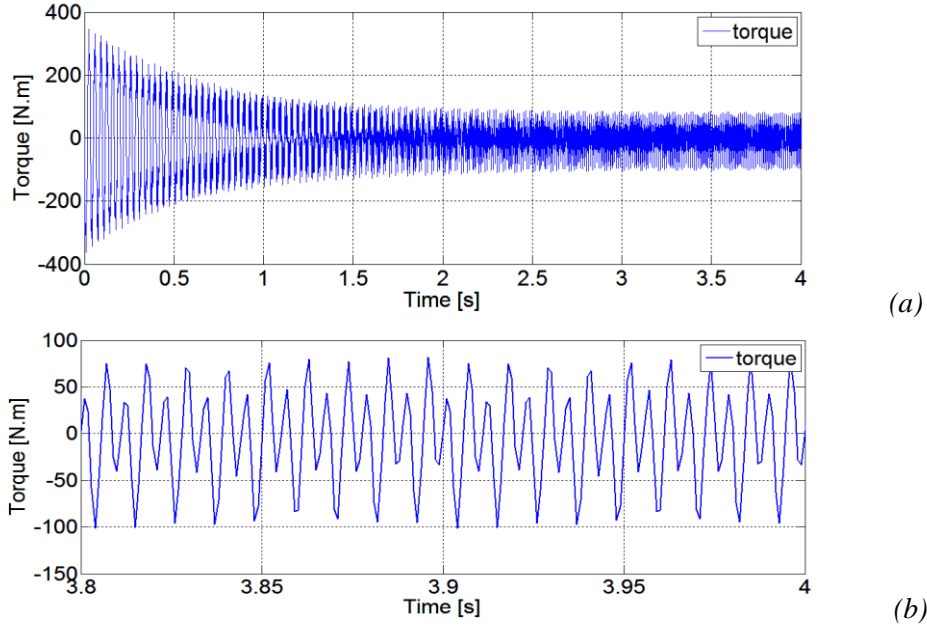


Figure 11. Torque variation at 300 rpm during (a) Total simulation time and (b) Detailed overview from last part.

### 3.7. Rate of Ripple Torque Wave

Some applications require a couple with a minimum of undulations. We try to minimize these undulations caused by the structure studied. The ripple rate is defined as Eq. (14):

$$\tau(\%) = \frac{\Gamma_{\max} - \Gamma_{\min}}{\Gamma_{\text{moy}}} \cdot 100 \quad (14)$$

We consider a parameter that allows us to reduce the ripple rate of the torque i.e angular spreading of the magnet in order. The undulations of the torque are due to the structure of the machine and the waveform of the supply current. Fig. 12 shows that the corrugations of the torque are related to those of the expansion torque. The minimum ripple of the resulting torque corresponds to angular spreading of the magnets of 50%.

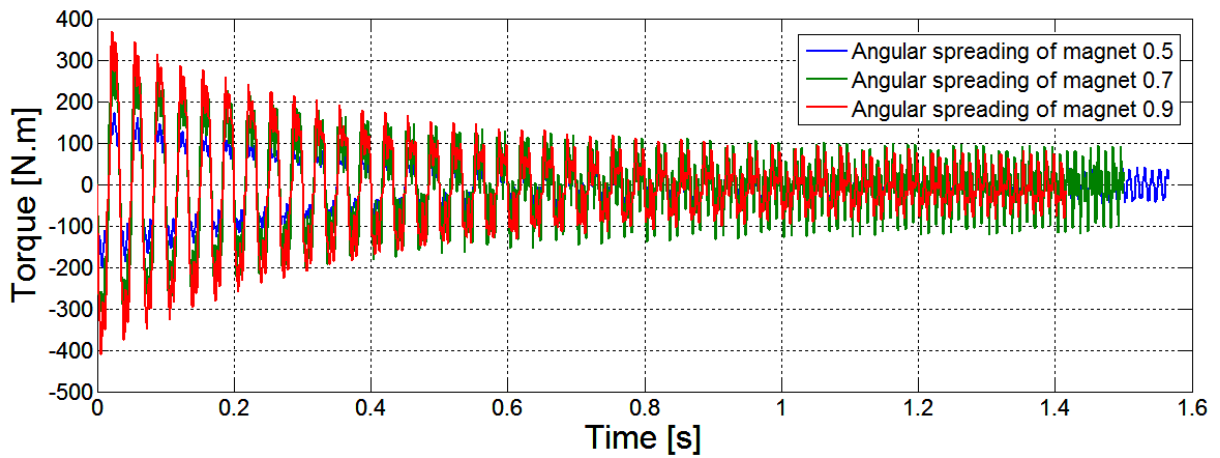


Figure 12. Torque variation at 300 rpm for different angular spreading of magnet.

## 4. CONCLUSIONS

In the present study, a new PM motor design has been presented. The magnetostatic and transient FEA findings have proven that the 3-phase motor is promising for its torque and current values for lower electrical loads. The magnetostatic findings have also proven that the stator core teethes are optimized for 0.5 mm. The new machine can be excited by three phases. The average torque value has been calculated as 65 Nm for no-load case. The presence of the harmonic must be carefully considered during the machine design process in order to minimize their impact on performance analysis. Various techniques are available for minimizing these undesirable effects, but such topics fall beyond the extent of this study.

## REFERENCES

- [1] Kurt, E., Gör, H., & Döner, U, “Electromagnetic design of a new axial and radial flux generator with the rotor back-irons”, *International Journal of Hydrogen Energy*, 2016, 41(17), 7019-7026. <<http://www.sciencedirect.com/science/article/pii/S0360319915314804>>.
- [2] Kurt, E, Gör, H & Demirtas, M, “Theoretical and experimental analyses of a single phase permanent magnet generator (PMG) with multiple cores having axial and radial directed fluxes”, *Energy Conversion Management*, 2014, 77, 163-172. <<http://www.sciencedirect.com/science/article/pii/S0196890413005505>>.
- [3] Xu, L., Ye, L, Zhen L.,& El-Antably, A, “A new design concept of permanent magnet machine for flux weakening operation”, *IEEE Transactions on Industry Application*, 1995, 31(2), 373-378. <<http://ieeexplore.ieee.org/abstract/document/370287/>>.
- [4] Gan, J., Chau, K. T., Chan, C. C., & Jiang, J. Z, “A new surface-inset, permanent-magnet, brushless DC motor drive for electric vehicles”, *IEEE Transactions on Magnetics*, 2000, 36(5), 3810-3818. <<http://ieeexplore.ieee.org/abstract/document/908381/>>.
- [5] Cheng, M., Chau, K. T., & Chan, C. C, “Design and analysis of a new doubly salient permanent magnet motor”, *IEEE Transactions on Magnetics*, 2001, 37(4), 3012-3020. <<http://ieeexplore.ieee.org/abstract/document/947054/>>.
- [6] Gör, H., & Kurt, E, “Preliminary studies of a new permanent magnet generator (PMG) with the axial and radial flux morphology”, *International Journal of Hydrogen Energy*, 2016, 41(17), 7005-7018. <<http://www.sciencedirect.com/science/article/pii/S0360319915312878>>.
- [7] Li, C., & Meng, T, “A new design concept of PMSM for flux weakening operation”, 19th International Conference on Electrical Machines and Systems (ICEMS), November 2016, 1-5.
- [8] Fernandez-Gamiz, U, Demirci, M, İlbaş, M, Zulueta, E, Ramos, J.A, Lopez-Guede, J.M, Kurt, E, “Computational characterization of an axial rotor fan”, *Journal of Energy Systems*, 2017; 1(4):129-137.
- [9] Collocott, S. J., J. B. Dunlop, P. B. Gwan, B. A. Kalan, H. C. Lovatt, W. Wu, & P. Watterson. “Applications of rare-earth permanent magnets in electrical machines: from motors for niche applications to hybrid electric vehicles”, In *China Magnet Symposium*, 2004, Xian, China, 2004.
- [10] Jahns, T, “Getting rare-earth magnets out of Ev traction machines: a review of the many approaches being pursued to minimize or eliminate rare-earth magnets from future EV drive trains”, *IEEE Electrification Magazine*, 2017, 5(1), 6-18. <<http://ieeexplore.ieee.org/abstract/document/7873383/>>.
- [11] Qiao, Z., Pan, S., Xiong, J., Cheng, L., Lin, P., & Luo, J., “Electromagnetic and microwave-absorbing properties of plate-like Nd–Ce–Fe powder”, *Journal of Electronic Materials*, 2017, 46(1) 660-667. <<http://link.springer.com/article/10.1007/s11664-016-4958-7>>.
- [12] Cavagnino, A., Lazzari, M., Profumo, F., & Tenconi, A, “A comparison between the axial flux and the radial flux structures for PM synchronous motors”, *IEEE Transactions on Industry Applications*, 2002, 38(6), 1517-1524. <<http://ieeexplore.ieee.org/abstract/document/1058105/>>.
- [13] Arslan, S & Kurt, E, “Design optimization study of a torus type axial flux machine”, In: *ECRES 2017*, 5. European Conference on Renewable Energy Systems; 27-30, August 2017: Vizeyon Publishing House, pp. 1-9.
- [14] Zhao, C., & Zhu, H, “Design and analysis of a novel bearingless flux-switching permanent magnet motor”, *IEEE Transactions on Industrial Electronics*, 2017. <<http://ieeexplore.ieee.org/abstract/document/7878553/>>.

- [15] Faiz, J., Valipour, Z., Shokri-Kojouri, M., & Khan, M.A, “Design of a radial flux permanent magnet wind generator with low coercive force magnets”, 2<sup>nd</sup> International Conference on Intelligent Energy and Power Systems (IEPS), IEEE, 2016 (pp. 1-7).
- [16] Park, H. J., Woo, D. K., Jung, S. Y., & Jung, H. K, “Modeling and analysis of magnet skew in axial flux permanent-magnet motor via field reconstruction method”, In Electrical Machines and Systems (*ICEMS*), IEEE, 2016, 19th International Conference on, pp. 1-4.
- [17] Vrtič, P., Vražić, M., & Papa, G, “Design of an axial flux permanent magnet synchronous machine using analytical method and evolutionary optimization”, *IEEE Transactions on Energy Conversion*, 2016, 31(1), 150-158. <<http://ieeexplore.ieee.org/abstract/document/7277061/>>.
- [18] Hemeida, A., Taha, M., Abdallah, A. A. E., Vansompel, H., Dupré, L., & Sergeant, P, “Applicability of fractional slot axial flux permanent magnet synchronous machines in the field weakening region”, *IEEE Transactions on Energy Conversion*, 2017, 32(1), 111-121. <<http://ieeexplore.ieee.org/abstract/document/7577790/>>.
- [19] A. M. El-Refaie & T. M. Jahns, “Impact of winding layer number and magnet type on synchronous surface PM machines designed for wide constant-power speed range operation”, *Energy Conversion, IEEE Transactions on Industrial Electronics*, 2008, 23, 53-60. <<http://ieeexplore.ieee.org/abstract/document/4025413/>>.
- [20] Tangudu, Jagadeesh K., & Thomas M. Jahns, “Comparison of interior PM machines with concentrated and distributed stator windings for traction applications”, *Vehicle Power and Propulsion Conference (VPPC)*, 2011, IEEE. <<http://ieeexplore.ieee.org/abstract/document/6043171/>>.
- [21] Di, Tommaso, A. O., Mastromauro, R., Miceli, R., Rizzo, R., & Viola, F, “Cogging torque comparison of interior permanent magnet synchronous generators with different stator windings”, 6<sup>th</sup> International Conference on Clean Electrical Power (ICCEP), IEEE, 2017. <<http://ieeexplore.ieee.org/abstract/document/8004780/>>.
- [22] Andrews, R. M., & Andreas, M., “Lorentz force in filtration of fibrous preforms”, *Metallurgical Transactions A*, 1991, 22(12): 2903-2915. <<http://link.springer.com/article/10.1007/BF02650251>>.
- [23] Arslan, S., Fidanboy, H., Demirbas, S., Guven, M. E., & Kurt, E, “Investigation of current harmonics using FEM on different rotor types of PMSMs”, In *Information, Communication and Automation Technologies (ICAT)*, October 2011, XXIII International Symposium on ,pp. 1-7.
- [24] Sistaninia, M., Phillion, A. B., Drezet, J. M., & Rappaz, M, “Simulation of semi solid material mechanical behavior using a combined discrete/finite element method”, *Metallurgical and Materials Transactions A*, 2011, 42(1), 239-248.
- [25] Rao, MV, Rama, Robert, L. Mullen, & Rafi L. Muhanna, “A new interval finite element formulation with the same accuracy in primary and derived variables”, *International Journal of Reliability and Safety*, 2011, 3(4): 336-357. <<http://www.inderscienceonline.com/doi/abs/10.1504/IJRS.2015.072716>>.
- [26] Neorem Magnets Co., Technical manual, (2003).
- [27] Kurt, E & Gor, H, “Electromagnetic design of a new axial flux generator”, 6<sup>th</sup> international conference electronics, computer and artificial intelligence ECAI, Oct 2014, in: *IEEE proc*, pp.39-42.
- [28] Benakcha . M, Benalia, L, Ameur. F, Tourqui . D. E, “Control of dual stator induction generator integrated in wind energy conversion system”, *Journal of Energy Systems* 2017, 1(1), 21-31. <<http://dergipark.gov.tr/jes/issue/30882/331059>>.
- [29] Rocha, J. E., & C. Sanchez, “The energy processing by power electronics and its impact on power quality”, *International Journal of Renewable Energy Development*, 2012, 1.3, 99.